Tutor

Dr. Francesc Viñes Solana
Departament de Ciència de Materials i Química Física

Grau de Química

Treball Final de Grau

Probing CO Adsorption on *fcc* Metals
Adsorció de CO en Metalls *fcc*

Lorena Pelegero Alonso

June 2019

Universitat de Barcelona

B:KC Barcelona Knowledge Campus
Campus d'Excel·lència Internacional

Aquesta obra esta subjecta a la llicència de:
Reconeixement–NoComercial-SenseObraDerivada

http://creativecommons.org/licenses/by-nc-nd/3.0/es/

“En la vida no existe nada que temer, solo cosas que comprender”.

Marie Curie

REPORT

CONTENTS

1. SUMMARY

The computational study on CO adsorption on coinage (Cu, Ni, Ag, Au) and Pt group (Pt, Pd, Ir, Rh) metal surfaces is interesting due to their application in catalysis where CO can be a reagent intermediate, product, as well as a poison, or used as probe molecule to charactize the metal surfaces transformation reactions. All these metals show a cube-shaped crystalline structure centered on the faces (*fcc*) where the most stable surfaces belong to the lowest Miller index — (100), (110), (111). We studied the CO stability on the different metal surfaces, so as to determine which position and conformation is the most stable, including upright and flat conformations, and different surface sites, with the aim of analysing the bond.

The study, carried out using Density Functional Theory (*DFT*) on slab models for the surfaces, and using the Perdew-Burke-Emezrhof (*PBE*) exchange-correlaction functional reveals the strong position to adsorb CO, C-connected, in an upright position, although different sites can be occupied. The stronger the bond, the close the CO to the surface, and the longer the CO bond elongates. Apparently, the adsorption is influential by the surface coordination number and surface energy. Accordingly, the surface bond measures the CO bond, reducing its ν(CO) stretching frequency whose values is quite connected to the surface connectivity, being Top>Bridge>Hollow. The different occupancy may help distinguishing different types of CO, oven surfaces. The strong nobility of Ag and Au, and the poisoning by CO of Pt group metals is also understood base on the computed adsorption energies.

Keywords: CO, Transition Metals, Density Functional Theory, Adsorption Energies, Catalysis, IR, Spectroscopy.

2. RESUM

L'estudi computacional de l'adsorció del monòxid de Carboni en superfícies tant de metalls nobles (Cu, Ni, Ag, Au) com d'alguns metalls del grup Pt (Pt ,Pd, Ir, Rh), és interessant per la seva aplicació en la catàlisi on el CO pot ser tan un reactiu intermedi, un producte, com un verí, o utilitzat com a molècula de sonda per caracteritzar les reaccions de transformació de les superfícies metàl·liques. Tots aquests metalls presenten una estructura cristal·lina de tipus cúbica centrada en les cares (*fcc*) on s'han utilitzat les superfícies més estables que corresponen als índex de Miller més baixos –(100), (110), (111). S'ha estudiat l'estabilitat del CO en les diferents superfícies metàl·liques per determinar en quina posició i conformació presenta més estabilitat, incloent les conformacions verticals i planes, i diferents llocs de superfície, amb l'objectiu d'analitzar l'enllaç.

L'estudi s'ha dut a terme utilitzant la Teoria Funcional de la Densitat (*DFT*) dels models de llesca (slab) per a les superfícies i emprant el funcional de correlació i intercanvi Perdew-Burke-Emezrhof (*PBE*), es revela que la posició d'adsorció més forta del CO, connectada a C, és en posició vertical, tot i que, poden ocupar llocs diferents. Com més fort és la interacció, el CO, més s'apropa a la superfície i més llarg és l'enllaç del CO. Pel que sembla, l'adsorció es troba influenciada pel nombre de coordinació superficial i l'energia superficial. En conseqüència, l'enllaç de la superfície mesura l'enllaç del CO, reduint la seva freqüència d'estirament ν(CO) on els valors estan bastant connectats per la interacció superficial, sent Top> Bridge> Hollow. La diferent ocupació pot ajudar a distingir diferents tipus de CO, en les superfícies. La forta noblesa d'Ag i Au, i l'enverinament del CO dels metalls del grup Pt s'explica també a partir de les energies d'adsorció computacionals.

Paraules clau: CO, Metalls de Transició, Teoria Densitat Funcional, Energies d'adsorció, Catàlisis, IR, Espectroscòpia.

3. INTRODUCTION

Late Transition Metals (*TMs*), including coinage (Cu, Ni, Ag, Au) and Pt-group (Pt, Pd, Ru, Rh, Ir, Os) metals are used in a large diversity of technological fields, from battery electrodes to electric contacts in circuits, up to jewellery. In heterogeneous catalysis they are normally used as catalytic active phases, given their moderate chemical activity, a direct consequence of their large stability, historically regarded as nobility. This normally implies that, on the curse of a catalysed process, the adsorption of reactants, reaction intermediates, and products, plus their diffusion, and the surface reaction energy barriers are moderate, being ideal catalysts according to *Le Sabatier* principle.[1]

A vital aspect of the research addressed at improving these late TMs catalysts activity/selectivity is acquiring an atomistic knowledge of their surfaces, including geometric and electronic structures, and how these affect the chemical activity, seized by the interaction strength with respect reagents, intermediates, and products. Such knowledge can be gained by studying well-defined catalysts, such as single crystal surfaces, at well-defined conditions, *e.g.* in ultrahigh vacuum conditions and a controlled temperature, and applying a series of complementary high-resolution surface science techniques studying the adsorption of simple, well-understood probe molecules. However, such studies are not always at hand, and even the detailed information is taken in averaged, mean terms. In the last decades, though, the acquisition of this knowledge has been possible thanks to the advent of accurate first-principles simulations, and the rise of the computational power, palpable in the available high-parallel supercomputing facilities, such as Marenostrum IV.

From the collection of probe molecules, carbon monoxide (CO) could be regarded as one of the main exponents for different reasons; but mostly because the adsorption conformation of CO is well-characterized, normally adsorbed connected upright of the metal surface connected through its C atom. This means that the specific surface area measurements of a metal/support catalysts can be based on the selective CO adsorption on the metal, once the CO adsorption conformation and the metal/CO ratio are known. Further than that, CO is involved as reagent, intermediate, or product for a series of technologically relevant reactions, *e.g.* the Fischer-

Tropsch (*FT*) process, in which a mixture of CO and H_2 are converted into liquid hydrocarbons, and catalysed normally by metals,[2]

$$n\mathrm{CO} + 2n\mathrm{H_2} \rightarrow \mathrm{C_nH_{2n}} + n\mathrm{H_2O} \quad (1),$$

also important for the FT process is the Water Gas Shift (*WGS*) reaction, which is a key process to stabilize the H_2/CO ratio in FT.[3]

$$\mathrm{CO} + \mathrm{H_2O} \rightarrow \mathrm{CO_2} + \mathrm{H_2} \quad (2).$$

This adjustment of the H_2/CO ratio is as well very important for other many reactions, including the methanol synthesis process, usually pursued on a Cu/ZnO catalyst,[4] but useful as well on the ammonia synthesis.[5]

$$\mathrm{CO} + 2\mathrm{H_2} \leftrightarrow \mathrm{CH_3OH} \quad (3),$$

$$\mathrm{N_2} + 3\mathrm{H_2} \leftrightarrow 2\mathrm{NH_3} \quad (4).$$

Furthermore, the Reverse WGS (*RWGS)* reaction is a way to get useful CO from CO_2, enabling a path to reuse greenhouse effect CO_2, and, by that, helping in fighting the climate change and global warming, and, eventually, turning the CO_2 waste into a used product.

Aside from the previous uses, the CO adsorption can be a poison, *e.g.* inhibiting the hydrogen function in fuel cells,[6] resulting in the requirement of a limiting concentration of CO in the used Pt-based catalysts,[7] yet this problematic appears as well on proton exchange membrane and direct alcohol fuel cells as used on electrical vehicles and other portable devices. However, the investigation of the CO adsorption on such TM surfaces by *ab initio* methodologies is by no means easy, nor exempt of inaccuracies. Large steps have been accomplished by using slab periodic models instead of cluster models[8] to simulate surfaces and the rise of first-principles Density Functional Theory (*DFT*) simulations has been key towards the description based on realistic models with sufficiently good degrees of accuracy. Still, standard DFT can yield inaccurate descriptions, such as the CO adsorption on hollow sites of Pt(111) surface, when it is experimentally know to adsorb on top of surface Pt atoms, a discrepancy known as the CO/Pt (111) puzzle.[9] For this particular case, a localized treatment of the metal electron density through the employment of hybrid exchange-correlation (*xc*) functionals and on the addition of a description for dispersive forces corrects/helps the duly description, although the use of hybrid functionals is unadvised in the description of TM bulks

and surface properties,[10] where other *xc* functionals, such as the Perdew-Burke-Ernzerhof (*PBE*), is recommended in general terms.

In the present project we aim at evaluating the accuracy of PBE in describing the CO adsorptive energetic, geometric, and vibrational properties when adsorbed on late TMs. To this end, the CO molecule will be adsorbed on high-symmetry positions on the low-Miller indices (001), (011), (111) surfaces of all late TMs displaying a face-centered cubic (*fcc*) crystallographic structures; Cu, Ni, Rh, Pd, Ag, Ir, Pt, and Au, as shown in Figure 1, given that these surfaces are the most stables surfaces normally exposed in the TM nanoparticles Wulff shapes, minimizing the overall surface tension.

	VIII	IX	X	XI	XII
3*d*	Fe	Co	**Ni**	**Cu**	Zn
4*d*	Ru	**Rh**	**Pd**	**Ag**	Cd
5*d*	Os	**Ir**	**Pt**	**Au**	Hg

Figure1. Section of the *d*-block of the periodic table, from groups VIII-XII, shaving coloured in red these cases under study

The results obtained on these surfaces are to be compared to available experimental data found in the literature, thus validating/refusing the utilization of PBE in the description of such a technologically important adsorptive system on TM surfaces. In addition, the infrared (IR) spectra are to be simulated, so as to gain information on the CO bonding with respect the surface.

4. OBJECTIVES

The objective of this work is to determine the most stable adsorptive interactions of CO on the most stable (001), (011), and (111) surfaces of *fcc* TMs by means of DFT optimizations on slab models, evaluating the accuracy of PBE *xc* functional in describing these ones, and comparing the geometric, energetic, and vibrational properties to available experimental results as well as to gain insights of the CO bonding through descriptors and trends along series and groups, and by the simulation of IR spectra. The specific objectives are then

- To find the most stable adsorptions of each surface and TM, considering different connectives, including upright and planar conformation situations.
- To compare adsorption trends through the TMs groups and series.
- To investigate the surface activity CO trends by correlating the adsorption energy trends towards surface chemical descriptors.
- To quantify the PBE accuracy on adsorption strengths, geometries, and vibrational frequencies comparing to experimental data.
- To simulate the IR spectra for the most stable geometries and analyse the CO bonding based on these.

5. THEORY

5.1. SCHRÖDINGER EQUATION AND HARTREE-FOCK

Quantum chemistry grounds in the resolution of the Schrödinger equation, a complex differential equation, first-order partial derivative in time, which indicates that the state of a system in a moment *t* is completely determined by the initial state Ψ (*t* = *Φ*) and a Hamiltonian (Ĥ)

$$i\hbar \frac{\partial \Psi_t}{\partial t} = \hat{H}\Psi_t \quad (5),$$

where the time-independent Schrödinger equation simplifies to:

$$\hat{H}\Psi = E\Psi \quad (6).$$

One of the approaches for solving this equation is the Born-Oppenheimer (*BO*) approximation, which relies on the fact that the relative mass of the nuclei is much higher than the electrons ones. This implies that the kinetic energy of the electrons is not affected by the nuclei, the kinetic energy of the nuclei is zero, and their repulsion a constant for a given configuration. Therefore, an electronic Hamiltonian can be determined with the following equation.

$$\hat{H}_{elec} = \hat{T}_e + \hat{V}_{ee} + \hat{V}_{en} \quad (7).$$

In computational physics and chemistry, the Hartree-Fock (*HF*) method is an approximation for the resolution of Schrödinger equation, that, when applying the $\hat{H}_{elec}$, determines the wavefunction and the energy of a quantum many-body system in a stationary state, through an iterative scheme. The HF method assumes that the wavefunction can be approximated by a single Slater determinant made of single electronic spinorbitals. Each solution (Ψ_{el} and E_{el}) represents an electronic state and, for each of these, one proceeds to the study of the movement of the nuclei by solving the corresponding nuclear Schrödinger equation,

$$\hat{H}_{nuc}\Psi_{nuc} \equiv E\Psi_{nuc} \quad (8),$$

$$\hat{H}_{nuc} = \hat{T}_{nuc} + \hat{V}_{nn} \quad (9).$$

The quantum wavefunctions methods, such as the HF and all post-HF methodologies can be quite accurate. For instance, the Coupled Cluster with Single, Double, and Triples, CCSD(T), is regarded as the golden standard in quantum simulations. However, the computational costs of these methods can be quite expensive, even prohibitive. This is the reason why other methods are sought, able to yield accurate results with a balanced computational cost.

5.2. DENSITY FUNCTIONAL THEORY

DFT is an alternative first-principles computational quantum mechanics method used in physics, chemistry, and materials science, and extendedly used to investigate the electronic structure of many-body systems, in particular atoms, molecules, and condensed phases. It has become a dominant tool simply because the computational costs are relatively low when compared to other wavefunctions methods, without compromising much the accuracy. DFT is based in that the energy of the ground state of a polyelectronic state depends solely, and gets determined by the electronic density function, ρ(r), and therefore, it is not necessary to know the wavefunction to describe the system. The electron density is defined as the electron probabilities all through space by the number of electrons, N.

$$\rho(r) = N \int \dots \int |\Psi(x_1, x_2, \dots, x_N)|^2 dx_1, dx_2, \dots, dx_N \quad (10),$$

Thus, a necessary requirement is that the number of electrons is gaited by the integration all through the space

$$\int \rho(r) dr = N \quad (11),$$

assuming as well that the electron density decreases to zero at infinite distance from nuclei.

$$\rho(r \to \infty) = 0 \quad (12).$$

5.2.1. The Hohenberg-Kohn theorems

Pierre Hohenberg and Walter Kohn in 1962 gave solidity to DFT with two theorems, known as the first theorem of Hobenberg-Kohn (*HK1*), and the second HK (*HK2*). HK1 is known as well as the existence and uniqueness theorem, and deals with the fact that the electronic density of the ground state, ρ_0(r), cannot come from two different external potentials, V_{ext}(r).

$$E_0 = E[\rho_0(r)] \quad (13).$$

This implies that the electron density is defined by the external potential, and *vice versa*.

$$\rho(r) \Leftrightarrow V_{ext}(r) \quad (14).$$

The HK1 provided one part of the fundamental theoretical basis for all modern variants of DFT. For any electronic system within an external potential, this is, the columbic potential generated by atomic nuclei at some given determined positions, the said potential determines —and can be determined— the ground state density. Hohenberg and Kohn showed that, for the ground state, there is a relationship between the electron density and the external potential, $V_{ext}(r)$. This means, that the electronic density in the ground state contains all the information of an electronic system; more details on the justification of this theorem can be found elsewhere.[11]

As a consequence of HK1, E is a functional of ρ(r), and can be expressed as,

$$E[\rho_r] = F[\rho_r] + \int \rho(r) v_{ext}(r) \quad (15),$$

where $F[\rho_r]$represents a universal function that contains the electronic kinetic energy, and the electronic interaction energy, $v_{ee}(\rho_r)$, as well within the BO approximation.

The second theorem of Hohenberg and Kohn, HK2, is also called the theorem of the variational principle, and deals with the fact that the energy of the ground state can be obtained variationally, and that the density that minimizes the total energy is indeed the exact electron density define by the external potential. Any density different from ρ_0, would deliver a higher energy.

$$E_0 \leq E[\rho] \quad (16).$$

5.2.2. The Kohn-Sham method

Walter Kohn y Lu Sham developed in 1965 a method to iteratively minimize the electron density of any given chemical system. For that, they required as a reference a fictitious system constituted by a homogeneous gas of non-interacting electrons. Within this system, the kinetic energy, corresponded to the sum of individual kinetic energies and the electronic density to the sum of orbital densities. Kohn Sham (*KS*) model included the electronic exchange and correlation as well. KS shared that a polyelectronic system described by a density ρ(r) could be replaced by this other system of non-interacting electrons with the same density ρ(r), In this way are could express the kinetic energy simply as,

$$\rho(r) = \rho_{KS}(r) = \sum_{i=1}^{N} |\Phi_i(r)|^2 \quad (17).$$

$$T_S[\rho] = \sum_{i=1}^{N} \langle \Phi_i | -\frac{1}{2}\nabla^2 | \Phi_i \rangle \quad (18),$$

and, actually, the system energy could be decomposed as a functional of the non-interacting system density according to

$$E \equiv T_s + E_{ext} + J + E_{xc} \quad (19),$$

where T_s is the electron kinetic energy, E_{ext} corresponds to the attraction of the external potential with the electron density, J is the Coulumb repulsion between electrons, and the last term E_{xc} is the difference between the real kinetic energy and the non-interacting system with respect the exchange and correlation (*xc*) energies.

All the terms are analytically known, except for E_{xc}, whose exact definition is unknown, which triggered different approximations to it. There are different types or families of such *xc* functionals, and their classification can follow the one proposed by Prof. John P. Perdew and called the Jacob's ladder.

5.2.3. Exchange and correlation functionals

The drawback of the KS method is that it is still inaccurate in the *xc* functionals; it is difficult to simulate in different chemical systems, including partially filled electron systems such as TMs, stretched bonds, or even Mott insulators[12]. For this reason functionals have been investigated and developed their type, as said, can be sorted according to the Jacob's Ladder, which consists of five rungs to improve the *xc* until reaching the exact one. Next, each rung is explained.

5.2.3.1. Local density approximation

The Local Density Approximation (*LDA*) is considered the first step of Jacob's ladder, and historically one of the most widespread strategies for the elaboration of *xc* functionals. LDA supposes that the density ρ_0(r) does not change practically with the position and assumes that it can be equated to the density of a system of a uniform and ideal electron gas, known as the Jellium system.[13]

$$E_{xc}^{LDA} = [\rho(r)] = \int f(\rho(r))\, dr \quad (20).$$

The advantage of LDA is that it describes the effects of *xc* through a real physical system and complies with the requirements of an universal relation, but the disadvantage is that it fails in describing certain systems in which there is a strong correlation. And is also known to yield

overbinding. For decades it has been extensively used to describe solid-state systems, even the adsorption of molecules, benefitting from this overbinding to compensate the lack of dispersive forces description, yielding accurate results, although for a wrong reason.

5.2.3.2. Generalized gradient approximation

The Generalized Gradient Approximation (*GGA*) is the second rung of Jacob's ladder, where the *xc* functional does not only depend on the value of the electron density at each point in space, but also on the density gradient, and can be summarized as

$$E_{XC}^{GGA}[\rho(r)] = \int f\big(\rho(r), \nabla\rho(r)\big)dr \quad (21).$$

Nowadays the GGA functionals are quite spread, also combined with dispersive forces treatments. Particularly, they have been found to be among the most accurate in describing TMs bulk and surface properties[14] as well as their electronic structure among functionals of the different Jacob's ladders rungs. Specially, the PBE *xc* functional is regarded as the best option in mean terms for TMs, and the one used in the present study.[15]

5.2.3.3. Meta-GGA functionals

The third step of Jacob's ladder is to add the kinetic energy density to the *ansatz*, *i.e*. the second derivative of ρ_0,

$$E_{XC}^{Metal-GGA}[\rho(r)] = \int f(\rho(r), \nabla(\mathrm{r}), \nabla^2(r))dr \quad (22)$$

The Meta-GGA functionals, such as the Tao-Perdew-Staroverov-Scuse (*TPSS*), imply normally an improvement on main group molecules thermochemistry, such as organic molecules, although it has been found to be detrimental for TMs.

5.2.3.4. Hybrid functionals

A fourth rung is normally assigned to hybrid functionals. It implies a linear combination of contributions of *xc* from LDA, GGA, or Meta-GGA, adding a part of HF exchange. Such functionals normally correct the self-interaction problem of the previous rungs of xc functionals, and help at localizing the electron density. It also represents an important step for main group molecules thermochemistry, but it is unadvised for delocalized systems such as metals.[16]

5.3. PERIODIC SOLIDS

A crystalline solid is a solid material with a highly ordered microscopic structure, forming a crystal lattice that extends in all directions of space. The periodicity of the crystal structure is

characterized by its primitive unit cell. The smallest group of particles in the material and their arrangement constitute the repeating pattern in the crystal. All the unit cells can be constructed from the primitive cell, but there is only one primitive cell, which is irreducible. Naturally, this structure contains the symmetry and structure of all the crystal in the three dimensions of space. The periodic pattern, also known as the Bravais lattice, is defined by three unit cell vectors, a_i, on which the translational operators $\hat{T}$ are constructed following

$$\hat{T} = n_1 a_1 + n_2 a_2 + n_3 a_3 \quad (23).$$

In this way, any point of the unit cell can be replicated whenever n_i correspond to full numbers, forming what is known as a crystalline structure. In the present work we will focus on face centered cubic (*fcc*) crystal structures, which is a close-packed arrangement of layers with ABC stacking, see Figure 2.

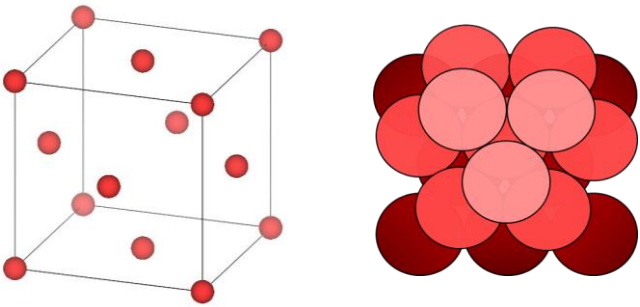

Figure 2. Unit cell of an fcc structure (left), red spheres represent the atoms. The ABC staking is shown with different shades of red (right).

5.3.1. Bloch theorem

The description of a crystal system can be treated on its unit cell, by adding the periodicity. To do so it is necessary to have a wavefunction that describes the unit cell under the crystal periodic boundary conditions. Therefore, when moving a point **r** to an equivalent point **r + R** of a replicated cell, are would need to meet the following expression.

$$\hat{T}\Psi(\mathbf{r}) = \Psi(\mathbf{r} + \mathbf{R}) = \Psi(\mathbf{r}) \quad (24),$$

i.e. the translational operator $\hat{T}$ yields the same value of the wavefunction when mood a full cell. This implies that the properties of the systems are periodic and given under the DFT by a periodic external potential $V_{ext}(r)$.

Bloch theorem explains that the electronic wavefunction is expressed as the product of a plane wave and another periodic function with the same periodicity of the crystal lattice.

$$\Psi_i(r) = e^{ikr} v_i(r) \quad (25).$$

In the above equation $\mathbf{k}$ represents a wavevector, and $v_i(r)$ the periodic function, which can be expressed as a linear combination of plane waves

$$\Psi_i(r) = \sum_G C_{i,k+G}\, G^{e^{i(k+G)r}} \quad (26).$$

Therefore, representing the wavefunctions of the real system as a plane waves sum of the reciprocal space becomes practical.

5.3.2. Reciprocal space

The reciprocal space is a space used for the study of solids according to Bloch theorem, related to Bravais network through;

$$b_i = 2\pi \frac{a_j \times a_k}{a_i \cdot (a_j \times a_k)} \quad \forall_{i,j,k} \in \{1,2,3\} \quad (27),$$

$$a_j \cdot b_j = 2\pi \delta_{ij} \quad (28).$$

There are infinite points in the reciprocal space, and so, one evaluates a discrete number of **k** vectors as defined in Block theorem, known as the **k**-points. Normally are defines a mesh of equidistant points, which can be reduced by symmetry reasons.

Note that the volume of the reciprocal space is inversely proportional to the direct space, that is, for small units cells many **k**-points are needed, yet for large cells the number of **k**-points can be reduced. Normally, one point is needed along directions having a vacuum region.

5.3.3. Miller indices

Vectors and planes in a crystal lattice can be described by the three-value Miller index notation.[17] These indices are defined from the smallest vector of the reciprocal network normal

to the plane. They are written (*hkl*) so to denote a family of planes, and the plane can be obtained using the following relation,

$$hb_1 + kb_2 + lb_3 \quad (29).$$

where *b,* are the reciprocal lattice vectors, where intersects with the real vectors a_i at x_1, x_2, and x_3:

$$x_1a_1 + x_2a_2 + x_3a_3 \quad (30).$$

The relationship between the Miller indices and the intersection points is:

$$h = \frac{1}{x_1}; k = \frac{1}{x_2};\ l = \frac{1}{x_3}; \quad (31).$$

For the case of simple cubic crystals, the lattice vectors are orthogonal and of equal length as are those of the reciprocal lattice. In the case of cubic systems, such as *fcc* crystals, the Miller indices surfaces of order 1 are the (001), (011), and (111) surfaces as shown in Figure 3.

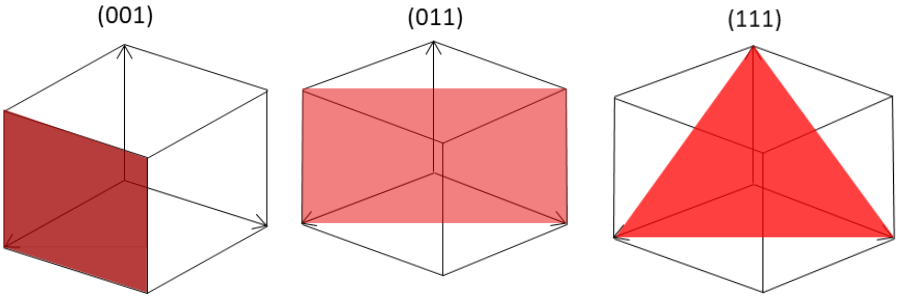

Figure 3. The (001), (011), and (111) lowest Miller indices surfaces for the fcc cubic crystalls, shown by color red planes.

5.3.4. Surfaces

The surfaces of the solids can be studied under periodic boundary conditions by means of the slab model, constructed from the unit cell and recreating it in the directions of the plane that one wants to study, but with a vacuum region orthogonal to it, see Figure 4. Normally 10 Å of vacuum is accurate enough for many systems, as interactions among replicated slabs are heavily reduced, and so negligible at these long distances.

The slab model must contain a series of layers, enough to correctly describe the electronic properties of the surface and the bulk. A non-symmetric slab can be formed where one side that represents the surface, is relaxed, white the other side is set to represent the bulk of the material.

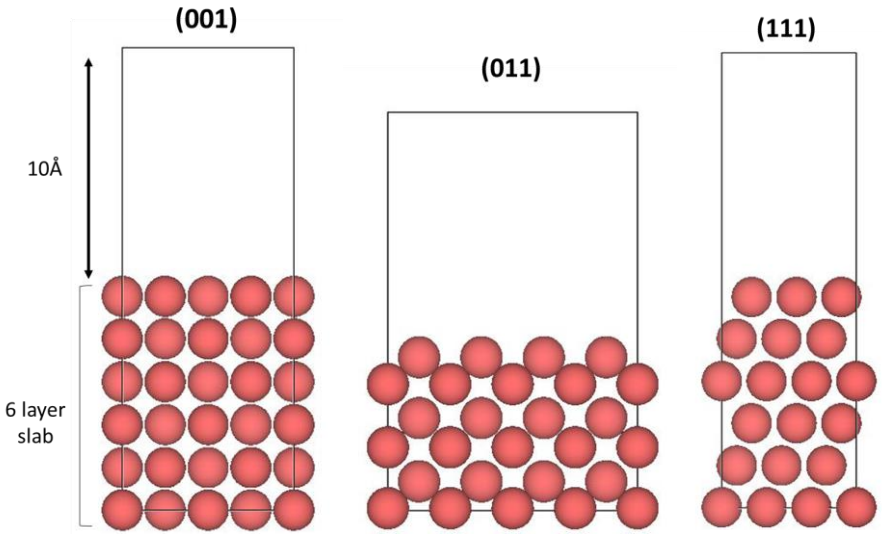

Figure 4. Side views of the slab models used for the studied three surfaces. Metal atoms are shown as red spheres.

5.4. INFRARED SPECTROSCOPY

Infrared (IR) spectroscopy is an extendedly used technique, in which molecules absorb IR light radiation that coincides with the vibrational frequencies of the molecules exciting them. For a vibration mode in a sample to be IR active it must imply a change in the molecular dipole moment. For molecules with N number of atoms, there are $3N-6$ vibrational modes potentially IR active, $3N-5$ for linear molecules, as the here studied CO. As commented, IR bands appear by the excitations of normal modes, which pass from the fundamental state that has the vibrational quantum number $\upsilon = 0$ to the first excited state that has the vibrational quantum number $\upsilon = 1$. There can also be direct transitions from the ground state to the second excited state $\upsilon = 2$, called overtones harmonic bands. Sometimes two modes are

similar in energy and close to the fundamental vibration, known as Fermi resonance, which is an especially strong anharmonic effect, which occurs between levels of combination with very close frequencies. Molecules can be regarded as linked atoms that vibrate continuously around positions of equilibrium. The vibrations can be very complex, but the theory of oscillatory movement has allowed to deduce that the combination of several very simple vibratory movements can be handled. The different movements of the molecules are sometimes represented as in Figure 5.

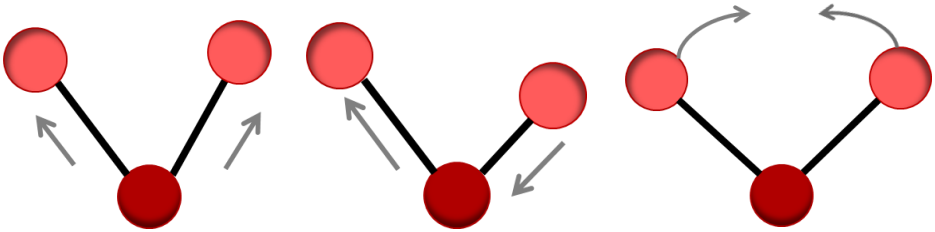

Figure 5. Typical vibratory movements of molecules: Symmetric stretching (left), asymmetric stretching (middle), and scissoring or bending (right).

Other vibrations can be asymmetric flexions in a plane (rocking), and symmetrical (wagging) and asymmetrical out-of-plane (twisting) movements. The CO case is simple, is that the only important vibration is just the stretching of the C=O double bond. The masses vibrate with characteristic frequencies that depend on them and the strength of the spring (k) according to the expression of classical physics:

$$\nu = \frac{1}{2\pi}\sqrt{\frac{k}{\mu}} \qquad (32),$$

$$\mu = \frac{M_1 M_2}{M_1 + M_2} \qquad (33).$$

The ν is the natural frequency of vibration; k is the force constant of the spring, that is, the bond, and μ is the reduced mass. The conclusions drawn from this expression are, on one hand, that the stronger or more rigid the chemical bonds is, the higher the frequency. On the other hand, the smaller atomic masses have a higher frequency.

5.4.1. Surface dipole selection rule

A selection or transition rule formally constrains the possible transitions of a system from one quantum state to another. In the case of vibrational excitations, they are IR active when imply a change in the molecule dipole moment. Thus, CO is IR retire. However, the situation changes when the CO molecule is adsorbed, e.g. on a metal surface. There, the substrate electron density may contact the dipole when the molecule lies flat, given the mirror centerdipole. However, the mirror centerdipole adds up to perpendicular dipoles, which are IR active, see Figure 6.

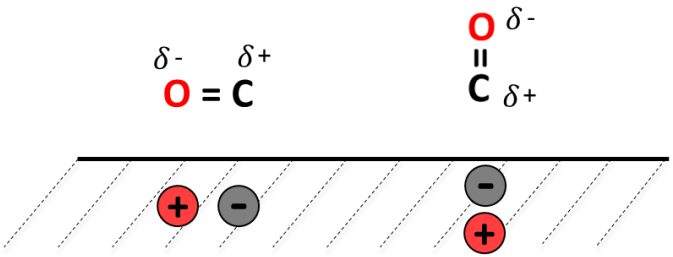

Figure 6. Effect of dipoles in the vacuum above the surface. Normal orientation (left) parallel orientation (right)

6. COMPUTATIONAL DETAILS

The DFT calculations have been performed using the Vienna *Ab Initio* Simulation Package (*VASP*)[18] using six-atomic layer slab models to simulate the TMs (001), (011), and (111) surfaces. A cutoff energy of plane wave basis is set of 415 eV has been used for the valence electron density, while the effect of the atomic cores on the valence electron density has been described using the Projector Augmented Wave (*PAW*) method.[19] To perform the calculations the three bottom layers of the slabs were kept fixed at the optimized geometry, while the other three upper layers were allowed to relax during the CO optimizations —*i.e.* 3+3 approach—. The reciprocal space has been sampled using a **k**-point Monkhorst-Pack mesh of 3×3×1 dimensions which has been found to be enough for accurate bulk calculations with variations in energies below 0.04 eV.[20]

The PBE *xc* functionals has been employed in the calculations. All the studied TM surfaces were modelled as six-layers slabs using either *p*(3×3) supercells for the (111) slab and (2×2) supercells for (001) and (011) slabs, thus having either 9 or 8 surface metal atoms, respectively, and, thus, modelling a similar surface coverage. These slab models contain a minimum of 10 Å of vacuum in between repeated slabs, yet in the case of Ni surfaces a large vacuum of 30 Å was added to avoid magnetic coupling. Optimizations were performed using a Gaussian smearing 0.2 eV energy width to improve convergence, yet final energies were extrapolated to 0 K. All calculations we carried out non spin-polarized, except for magnetic Ni surfaces and CO adsorbed upon. The reference isolated CO molecule has been optimized within an asymmetric cell of 9×0×11 Å dimensions and calculated at Γ point. The optimization critery was set to $10^{-5}$for electronic convergence, while forces on atoms were below 0.01eV· $Å^{-1}$for the ionic convergence. The frequency calculations were carried cut by finite displacements of 0.03 Å, constructing and diagonalizing the Hessian matrix.

7. RESULTS AND DISCUSSION

To determine the most stable adsorption site of CO on *fcc* metal surfaces, different CO orientations have been explored*, a)* CO perpendicular to the surface connected through the C atom, *b)* CO also perpendicular but connected through the O atom, and, finally, *c)* CO parallel to the surface plane as shown in Figure 7.

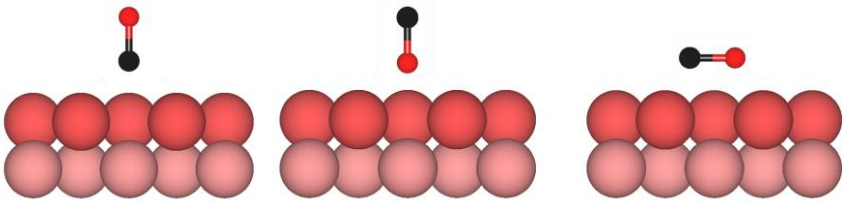

Figure 7. Initial orientation on the CO molecule, including a) perpendicular C-connected, b) perpendicular O-connected, and c) parallel to the surface.

Each mode has been made on the three (001), (011), (111) metal surfaces on highly symmetrical positions, including, Top (T), Bridge (B) and Hollow (H) positions, see figure 8, 9, and 10.

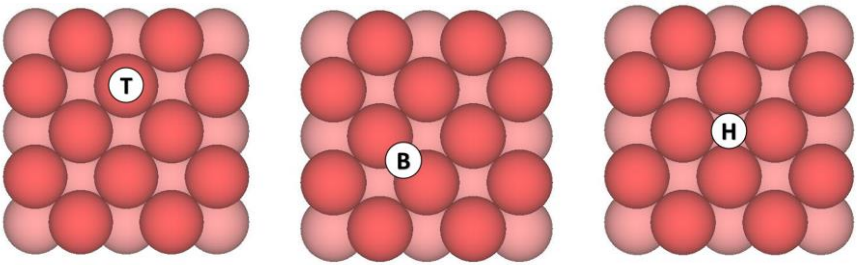

Figure 8. Top views of (001) Surface and the explored sites. The Surface layer is shown as red spheres and pink spheres for the second (subsurface).

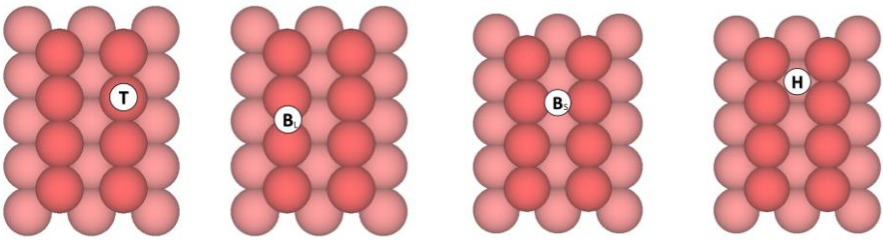

Figure 9. Top views of (011) Surface and the explored sites. The Surface layer is shown as red spheres and pink spheres for the second (subsurface).Top, Bridge long, B_L, Bridge short, B_S, and Hollow respectively.

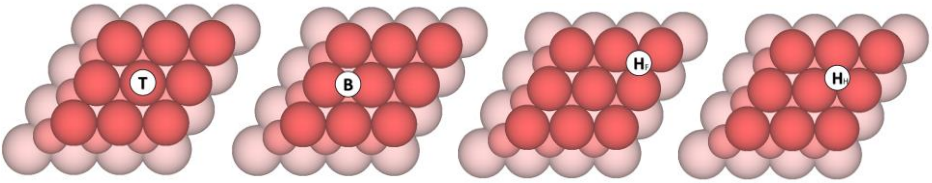

Figure 10. Top views of (111) Surface and the explored sites. The Surface layer is shown as red spheres and pink spheres for the second (subsurface), and pale pink for the third and more profund layers. Top, Bridge, Hollow *fcc,* H_f, and Hollow hexagonal close-packet *(hcp)* ,H_h, respectively

To obtain the adsorption energies of our systems we need to optimize the surface alone, the carbon monoxide molecule and the surface with the carbon monoxide so to get their energies, E_{Metal}, E_{CO}, and $E_{\mathrm{CO/Metal}}$ respectively. In this way, from the following equation, we obtained the final adsorption energies.

$$\mathrm{E_{ads}} = E_{\mathrm{S}} + E_{\mathrm{CO}} - E_{\mathrm{CO/Metal}} \qquad (34).$$

With this definition, the more positive the $\mathrm{E_{ads}}$, the stronger the binding. This systematic study it implies over 370 optimizations.

7.1. ADSORPTION ENERGY

After having optimized the previous structures the results obtained confirm that the upright position is always the most stable one, observing even that structure for flat CO molecules evolve upright. In addition, when the CO is bound by the Oxygen, obtained $\mathrm{E_{ads}}$, are near zero, at most, 20 $\mathrm{kJ \cdot mol^{-1}}$, and so have been discarded. In Table 1 summarizes the adsorption

energies, upright an C-connectes on the Top, Bridge, and Hollow positions in (001), (011), (111) surfaces.

$E_{ads}(kJ \cdot mol^{-1})$	Position	(001)	(011)	(111)
Cu	Top	82	86	63
	Bridge	82	$49^{BL}/91^{BS}$	63
	Hollow	76	1	$69^{Hf}/69^{Hh}$
Ag	Top	26	31	16
	Bridge	22	$27^{BL}/27^{BS}$	4
	Hollow	2	0	$2^{Hf}/1^{Hh}$
Au	Top	47	57	33
	Bridge	52	$21^{BL}/5^{BS}$	23
	Hollow	7	1	$16^{Hf}/16^{Hh}$
Ni	Top	165	164	145
	Bridge	182	$144^{BL}/179^{BS}$	171
	Hollow	189	127	$184^{Hf}/183^{Hh}$
Pd	Top	203	162	135
	Bridge	243	$166^{BL}/197^{BS}$	197
	Hollow	233	117	$119^{Hf}/197^{Hh}$
Pt	Top	187	211	170
	Bridge	210	$2^{BL}/216^{BS}$	181
	Hollow	158	2	$183^{Hf}/185^{Hh}$
Rh	Top	182	195	177
	Bridge	193	$154^{BL}/188^{BS}$	196
	Hollow	181	105	$196^{Hf}/188^{Hh}$
Ir	Top	210	237	197
	Bridge	195	$154^{BL}/200^{BS}$	174
	Hollow	163	56	$180^{Hf}/169^{Hh}$

Table 1. Adsorption energies, E_{ads}, in $kJ \cdot mol^{-1}$, for CO adsorbed on diverse high symmetry sites, being always upright and C-connected, on the (001), (011), and (111) surfaces of *fcc* TMs.

For the (001) surfaces the most stable position is Top on Cu, Ag, and Ir, Bridge for the Au, Pd, Pt, and Rh and Hollow for Ir. On the (011) surfaces the Top position is the most stable for Ag, Rh, and Ir, but B_S for Cu, Au, Ni, Pd, and Pt. Finally, on (111) surfaces the Top position is the

most stable for Ag, Au, and Ir, but Ni and Rh, while Hh for Cu, Pd, and Pt. As commented one sees here the deficiency of standard DFT PBE calculations on simulating Pt (111), where are would except the experimentally observed Top position.[15]

Figure 11, shows the trends in Top position for all surfaces, so as to get on unbiased comparison towards the metal surface, plus trends to be considered the expected, desirable adsorption site.

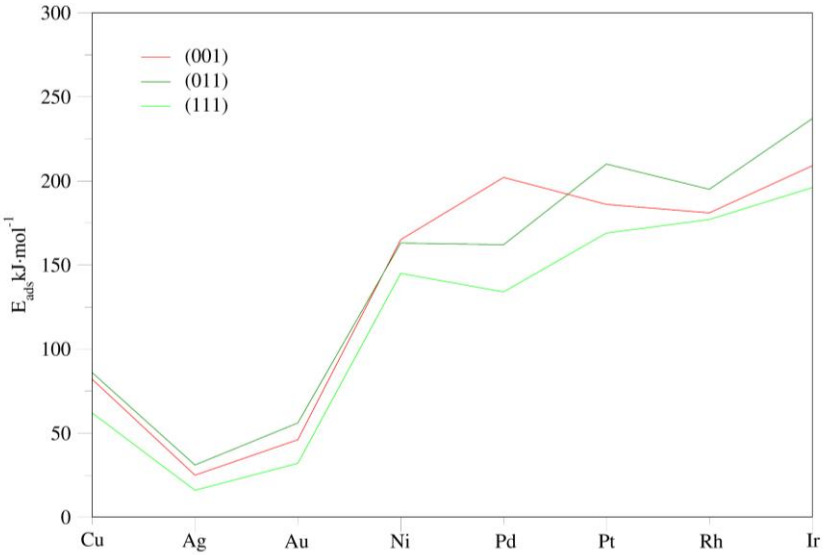

Figure 11. Evolution of E_{ads} of CO on Top positions on the different Miller indices surfaces of *fcc* TMs.

From the figure are clearly sees that the surface with the highest adsorption is (011). This correlates with it being the most unstable surface with highest surface energy, and low Condition Number (CN) of 7. On the other side the (111) surface. The most stable and highest CN, being 9, is the least active surface. Finally, the (001) surface, with CN=8 and moderate surface energies is placed in between. It is remarkable that the metals had interact with CO are Ag and Au, being these more noble than the rest. Here it is worth to highlight that Ag is more noble than Au when it comes to adsorbing CO, which differs with the common knowledge, but has been explained due to the fact that the Ag deeper *d*-band centre implies a weaker C-Ag coupling, which prevents antibonding states being above Fermi level, and so, destabilizing the C interaction towards Ag.[22]

Indeed, a descriptor of the *d*-band, the so-called, *d*-band center, E_d, is normally used to understand the chemical bonding on such late TMs. Indeed, are correlated the present E_{ads} vs E_d in Figure 12, showing a clear trend in that the lower the E_d, the largest the E_{ads}.

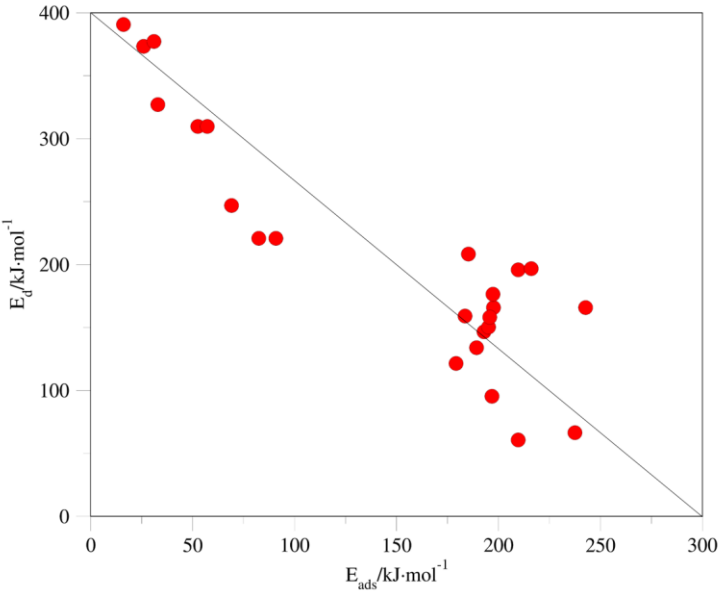

Figure 12. Correlation of E_{ads} with a descriptor E_d.

7.1.1. CO Bonding

Table 2 shows, for each studied case, the CO bond length. From the data it is clear that in many cases the values differ (elongate) from the bibliographic value being 1.14 Å and here, in vacuum, computed to be 1.14 Å. On the (001) and (111) surfaces and Top positions the elongations might be minimal, few times below 0.01 Å, while on Bridge site may alongside more, sometimes, 0.06 Å. On the (011) surface there is no remarkable trend with respect to positions. In any case, in general, the values show that the C=O bond elongates (weakens), when adsorbing on the TM surfaces; which may have influence on the vibrational frequency, see below.

d(CO) /Å	Position	(001)	(011)	(111)
	Top	1.16	1.14	1.16
Cu	Bridge	1.17	$1.15^{BL}/1.17^{BS}$	1.17
	Hollow	1.2	1.14	$1.15^{Hf}/1.15^{Hh}$
	Top	1.15	1.15	1.15
Ag	Bridge	1.16	$1.15^{BL}/1.16^{BS}$	1.16
	Hollow	1.14	1.14	$1.17^{Hf}/1.17^{Hh}$
	Top	1.15	1.15	1.15
Au	Bridge	1.17	$1.17^{BL}/1.17^{BS}$	1.17
	Hollow	1.18	1.14	$1.18^{Hf}/1.18^{Hh}$
	Top	1.16	1.17	1.16
Ni	Bridge	1.18	$1.21^{BL}/1.18^{BS}$	1.19
	Hollow	1.21	1.21	$1.19^{Hf}/1.19^{Hh}$
	Top	1.16	1.16	1.16
Pd	Bridge	1.18	$1.19^{BL}/1.18^{BS}$	1.19
	Hollow	1.2	1.19	$1.19^{Hf}/1.19^{Hh}$
	Top	1.16	1.16	1.16
Pt	Bridge	1.18	$1.50^{BL}/1.18^{BS}$	1.18
	Hollow	1.2	1.14	$1.19^{Hf}/1.20^{Hh}$
	Top	1.17	1.17	1.16
Rh	Bridge	1.18	$1.14^{BL}/1.19^{BS}$	1.2
	Hollow	1.21	1.2	$1.20^{Hf}/1.20^{Hh}$
	Top	1.16	1.17	1.16
Ir	Bridge	1.18	$1.20^{BL}/1.19^{BS}$	1.19
	Hollow	1.21	1.19	$1.20^{Hf}/1.20^{Hh}$

Table 2. CO bond lengths, *d*(CO), in Å, for each adsorption site studied.

7.1.2. MC Bonding

Table 3 shows the as created the M-C bond for each studied situation. The Top position has the smallest distance since the CO is adsorbed straight. The distance on Bridge and Hollows have been averaged between the metal atoms in contact. To do a fair comparison, and as an example, the E_{ads} and *d*(MC) are shown for Top positions of the other sites/surfaces. The results are shown in Figure 13.

d(MC) Å	Position	(001)	(011)	(111)
	Top	1.85	1.99	1.86
Cu	Bridge	1.99	$4.29^{BL}/1.97^{BS}$	1.99
	Hollow	2.15	4.11	$2.06^{Hf}/2.05^{Hh}$
	Top	2.15	2.13	2.17
Ag	Bridge	2.29	$4.49^{BL}/2.27^{BS}$	2.31
	Hollow	2.29	4.15	$2.38^{Hf}/2.38^{Hh}$
	Top	2.01	1.99	2.03
Au	Bridge	2.14	$4.50^{BL}/2.13^{BS}$	2.16
	Hollow	2.37	4.15	$2.27^{Hf}/2.25^{Hh}$
	Top	1.74	1.75	1.74
Ni	Bridge	1.88	$1.20^{BL}/1.87^{BS}$	1.88
	Hollow	2.04	2.25	$1.95^{Hf}/1.95^{Hh}$
	Top	1.87	1.87	1.87
Pd	Bridge	2.00	$3.01^{BL}/1.99^{BS}$	2.07
	Hollow	2.21	2.48	$2.15^{Hf}/2.07^{Hh}$
	Top	1.84	1.85	1.85
Pt	Bridge	2.01	$4.50^{BL}/2.01^{BS}$	2.03
	Hollow	2.26	3.81	$2.12^{Hf}/2.12^{Hh}$
	Top	1.85	1.86	1.84
Rh	Bridge	2.03	$4.39^{BL}/2.00^{BS}$	2.09
	Hollow	2.23	2.53	$2.09^{Hf}/2.10^{Hh}$
	Top	1.87	1.86	1.85
Ir	Bridge	2.07	$4.73^{BL}/2.03^{BS}$	2.05
	Hollow	2.29	4.65	$2.13^{Hf}/2.14^{Hh}$

Table 3. MC bond lengths, *d*(MC), in Å, for each adsorption site studied.

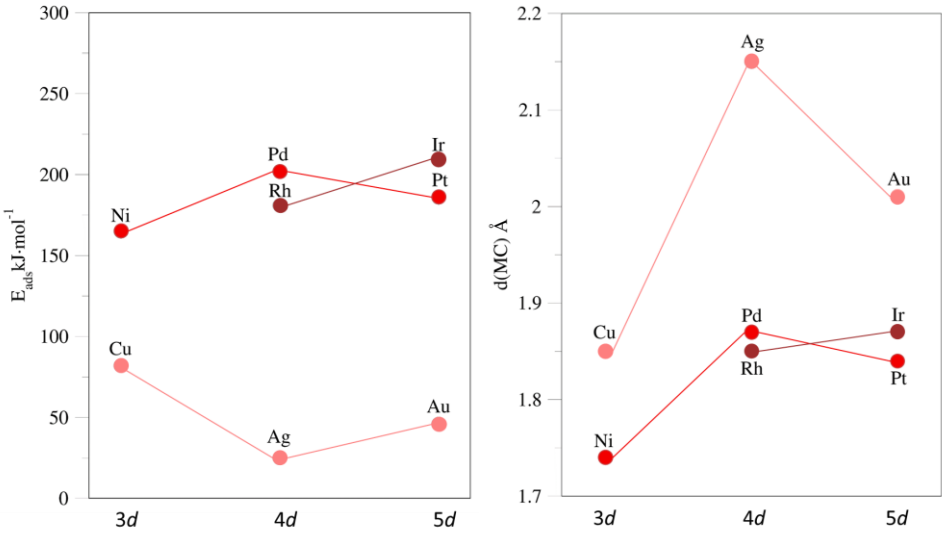

Figure 13. $E_{ads}(kJ \cdot mol^{-1})$ CO of (001) surfaces for TOP position and distances, in Å.

One clearly sees that noble metals, Cu, Ag, and Au, are those that have the smallest E_{ads} and, consequently, have larger *d*(MC) distances, due to the fact that being noble metals are more stable, interact less with CO, and, therebefore, the bond is weaker, and by that, longer. The other metals have higher E_{ads}, therefore, interact stronger with CO. This has many implications; noble metals could be ideal for CO conversion, adsorbing it moderately, and not being poisoned by CO, at variance with the rest of the studied metals, in accordance with the common abstention in catalysis. In any case, the adsorption of CO is straight, well-defined. And strong enough as to use it as probe molecule.

7.1.3. Height

Similar to *d*(MC), the height of the C atom yields similar conclusions, see table 4, here measured as the vertical distance of C with respect the mean positions of the high metal layer. According to this, the Top heights are almost identical to (MC), and, it any difference, comes from small metal layers rumpling occupying upon CO adsorption.

h /Å	Position	(001)	(011)	(111)
Cu	Top	1.85	1.99	1.86
	Bridge	1.67	$1.35^{BL}/1.59^{BS}$	1.59
	Hollow	1.20	3.45	$1.41^{Hf}/1.51^{Hh}$
Ag	Top	2.15	2.13	2.17
	Bridge	1.83	$2.09^{BL}/1.76^{BS}$	1.83
	Hollow	3.68	3.27	$1.64^{Hf}/1.70^{Hh}$
Au	Top	2.01	1.99	2.03
	Bridge	1.64	$1.45^{BL}/1.63^{BS}$	1.68
	Hollow	1.31	3.27	$1.42^{Hf}/1.52^{Hh}$
Ni	Top	1.74	1.75	1.74
	Bridge	1.54	$0.60^{BL}/3.37^{BS}$	1.49
	Hollow	1.09	0.75	$1.32^{Hf}/1.40^{Hh}$
Pd	Top	1.87	1.87	1.87
	Bridge	1.56	$1.70^{BL}/1.61^{BS}$	1.38
	Hollow	1.06	0.70	$1.48^{Hf}/1.38^{Hh}$
Pt	Top	1.84	1.85	1.85
	Bridge	1.58	$3.54^{BL}/1.67^{BS}$	1.60
	Hollow	1.12	3.02	$1.34^{Hf}/1.43^{Hh}$
Rh	Top	1.85	1.86	1.84
	Bridge	1.59	$3.43^{BL}/1.54^{BS}$	1.42
	Hollow	1.16	1.16	$1.34^{Hf}/1.46^{Hh}$
Ir	Top	1.87	1.86	1.85
	Bridge	1.62	$3.81^{BL}/1.55^{BS}$	1.60
	Hollow	1.24	0.96	$1.37^{Hf}/1.48^{Hh}$

Table 4. Height MC in Å for all the surfaces.

Here an exemplary comparison is made for the different sites on the (111) surfaces, see Figure 14. One can see that the Top position is the one with highest heights, mainly due to the straight contact. Hollow positions are those that present less *h* since they interact with atoms of the sublayer and that makes them closer to the surface on the Hollow, and so the same applies, to a longer extent, to Bridge sites. Here one sees a bit longer height for noble metals (Cu, Ag, Au), although less pronounced that the MC bond lengths.

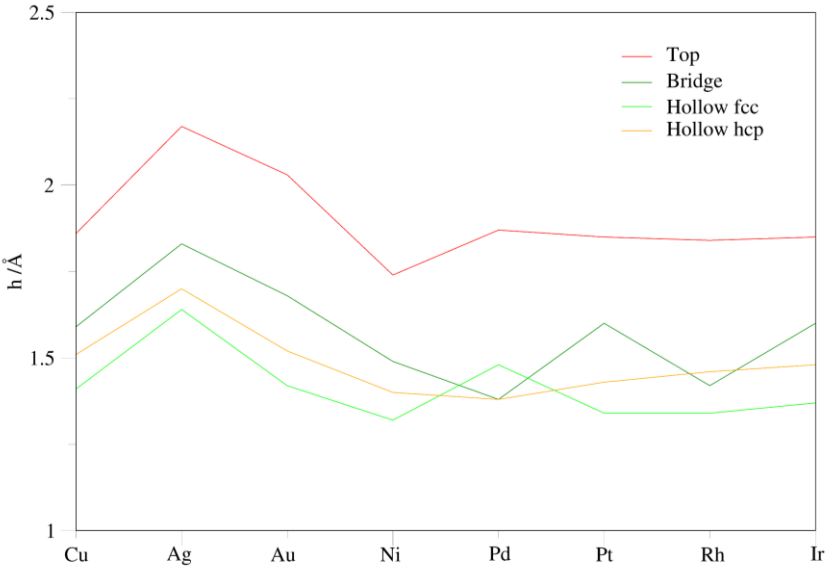

Figure 14. Height in Å for (111) surface in all positions.

7.2. INFRARED SPECTRA

Table 5 summarizes the $\nu(\mathrm{CO})$ stretching vibrations, for each studied situation. For the (001) surfaces the largest frequencies are observed for the Top positions in all the metals except for the Ag, where it is in the Hollow. On the (011) surfaces the highest frequencies belong to Hollow position for Cu, Ag, Au, and Pt, but Top for metals Ni, Pd, Ir. Finally, the B_L contains the largest frequencies for Rh. For the rest of metals, these are on Hollows. Thus, there is no closer trend or preference on the occupancy.

However, here is a clear trend in that, in general, $\nu(\mathrm{CO})$ Top > $\nu(\mathrm{CO})$ Bridge > $\nu(\mathrm{CO})$ Hollow. With that site consideration, and the different site preferences farther different graphs and surfaces, are could simulate the IR for each metal on the most stable sites, as shown in Figure 15.

$\nu\ /\mathrm{cm}^{-1}$	Position	(001)	(011)	(111)
Cu	Top	2024	2032	2033
	Bridge	1889	$2088^{L}/1904^{S}$	1886
	Hollow	1708	2127	$2093^{F}/2092^{H}$
Ag	Top	2044	2047	2050
	Bridge	1934	$2014^{L}/1944^{S}$	1939
	Hollow	2127	2124	$1902^{F}/1898^{H}$
Au	Top	2062	2067	2073
	Bridge	1884	$1895^{L}/1895^{S}$	1911
	Hollow	1749	2128	$1857^{F}/1842^{H}$
Ni	Top	2007	1994	2016
	Bridge	1852	$1570^{L}/1849^{S}$	1832
	Hollow	1638	1656	$1774^{F}/1772^{H}$
Pd	Top	2034	2021	2044
	Bridge	1874	$1803^{L}/1862^{S}$	1780
	Hollow	1691	1753	$1818^{F}/1775^{H}$
Pt	Top	2058	2040	2070
	Bridge	1853	$2127^{L}/1846^{S}$	1858
	Hollow	1685	2110	$1769^{F}/1759^{H}$
Rh	Top	1989	1966	2006
	Bridge	1842	$2129^{L}/1809^{S}$	1738
	Hollow	1656	1740	$1737^{F}/1754^{H}$
Ir	Top	2016	1980	2027
	Bridge	1845	$1711^{L}/1785^{S}$	1808
	Hollow	1656	1782	$1716^{F}/1728^{H}$

Table 5. Frecuencies, in cm^{-1}, for all the studied surfaces.

All adsorbed CO are active, yet the intensities may differ a bit, but being always of the same order. In many cases the CO on different surfaces are placed at different frequencies, that could enable their distinction in polycrystalline samples, or, viceversa, the identification of such exposed surfaces by CO probing. An exemplary case could be Rh, where CO prefers to adsorb Bridge on (001), Top on (011), and Hollow *fcc* on (111), with $\nu(\mathrm{CO})$ that differ by more than 100 cm^{-1} in each position. On the other hand, this distinction would be hardly feasible on Ag,

where, even having different adsorption sites Tops in (001), and (011), Hollow *fcc* in (111), the $\nu(\mathrm{CO})$ are too close to distinguish them, specially on (001) and (011) surfaces, being the difference only of 3 cm^{-1}.

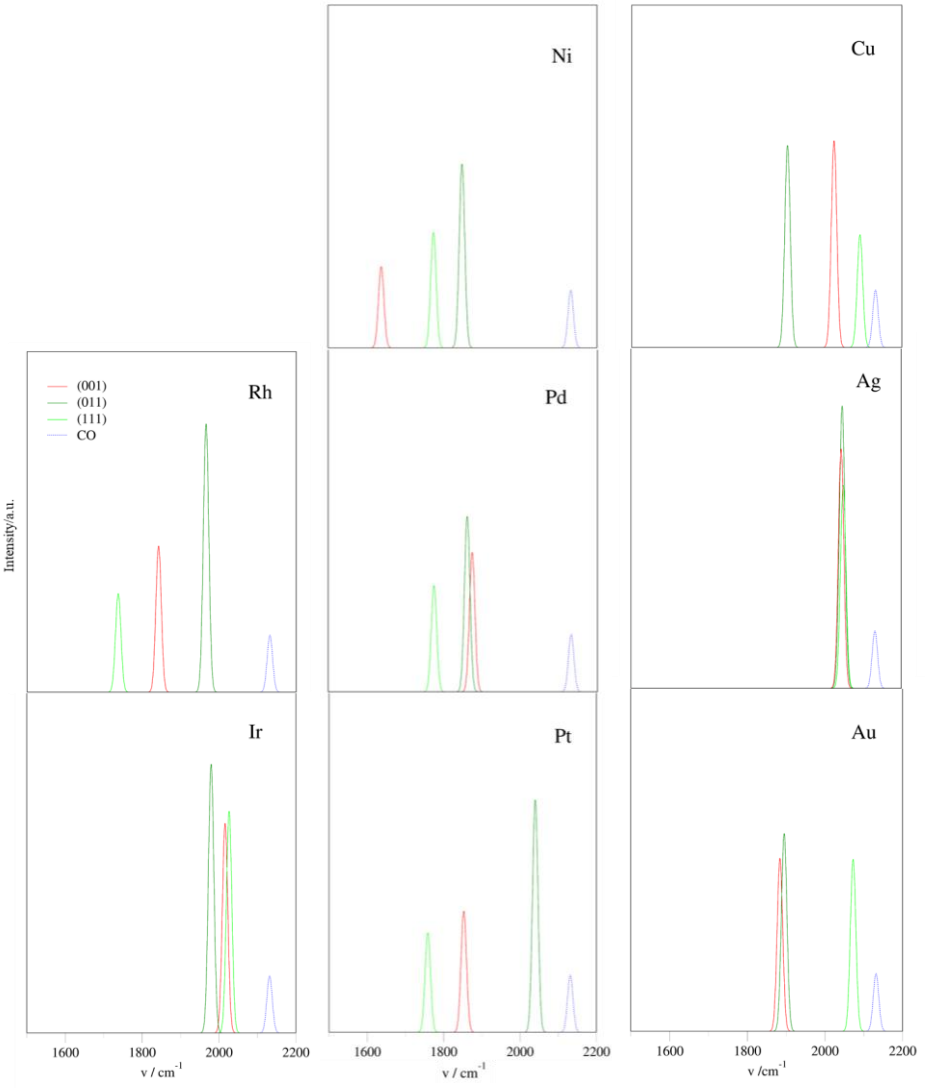

Figure 15. Simulated IR spectra TMs, all surfaces, in the most stable CO adsorption positions.

The difference intensity of the peaks is due to the fact that the larger change of the dipolar moment, the greater the intensity. We also observe that all the frequencies have values smaller than the CO in the gas phase, this is due to the fact that, when adsorbed on the surface, the CO bond has been weakened, because the CO molecule is linked by a double bond and contains a pair of free electrons, and, when approaching a metal the CO acts as a ligand forming a σ metal-carbon bond, so the carbon donates its pair of free electrons to the metal that is defective of electrons, but in turn, the metal delivers electrons to the CO π* orbitals, in the known phenomenon of retrodonation. Therefore, the higher the adsorption energy, the lower frequency we obtain, as exemplifier this is represented in the following Figure 16.

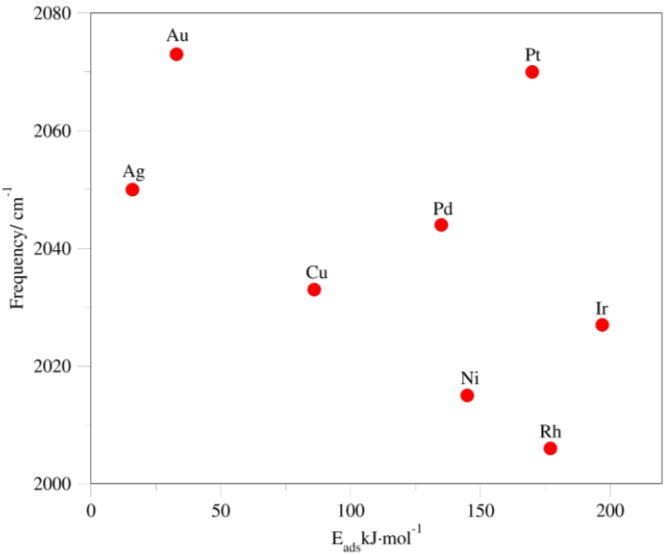

Figure 16. Correlation of frequencies vs E_{ads} for (011) surfaces, on the Top positions.

7.3. CALCULATION OF ERRORS.

To determine the calculation of errors, we searched in the bibliography for several values as here optimized in this work, see Table 6, in this way, we have been able to compare and thus determine the validity of the calculations through an statistic study, see Table 7.

TM Surface	Site	E_{ads}/kJ· mol^{-1}	*d*(CO)/Å	*h*/Å	ν/cm^{-1}
Ag (111)	Top	27[a]	1.15[f]	2.05[f]	2137[a]
Au (111)	Top	39[a]	1.16[f]	1.96[f]	—
Cu (111)	Top	41[a]	1.16[a]	1.91[a]	2072[a]
	Bridge	63[e]	—	—	—
	Hollow *fcc*	69[e]	—	—	—
	Hollow *hcp*	69[e]	—	—	—
Ni (111)	Top	175[g]	—	—	2044[a]
	Hollow *fcc*	130[a]	1.15[a]	1.34[a]	—
	Hollow *hcp*	124[a]	1.18[a]	1.29[a]	—
Pd (111)	Top	148[f]	1.16[f]	1.83[d]	—
	Hollow *fcc*	163[d]	1.14[a]	1.27[a]	1848[a]
	Hollow *hcp*	138[d]	1.15[a]	1.29[a]	1823[a]
Pt (111)	Top	163[b]	1.15[a]	1.85[d]	2100[a]
	Bridge	175[e]	—	—	1850[a]
	Hollow *fcc*	177[e]	1.20[b]	2.11[b]	1810[a]
	Hollow *hcp*	175[e]	1.16[b]	1.85[b]	1736[a]
Rh (111)	Top	145[a]	1.17[c]	1.83[c]	2000[c]
	Bridge	180[c]	1.19[c]	2.01[c]	1813[c]
	Hollow *fcc*	176[e]	1.20[c]	2.09[c]	1753[c]
	Hollow *hcp*	181[e]	1.20[c]	2.07[c]	1745[c]
Ir (111)	Top	175[a]	1.17[f]	1.88[d]	2063[a]
	Bridge	160[e]	—	—	—
	Hollow *fcc*	156[e]	—	—	—
	Hollow *hcp*	162[e]	—	—	—

Table 6. bibliographic values [a]Ref. 22; [b]Ref. 23; [c]Ref. 24; [d]Ref. 25; [e]Ref. 26; [f]Ref. 27; [g]Ref. 28

Error type	E_{ads}/kJ· mol^{-1}	*d*(CO)/Å	*h*/Å	ν/cm^{-1}
ME	-11	-0.01	0.17	26
MAE	20	0.02	0.26	33
MAPE	16	1.41	18.15	2

Table 7. Mean Error (*ME*), Mean Absolute Errors (*MAE*), and Mean Absolute Percentage Error (*MAPE*).

As seen in Table 7, the errors of *d*(CO) and *h* are minimal, and so, we can consider them optimal. The $\mathrm{E_{ads}}$ have a greater error, but the error of the DFT method; 10-20 $\mathrm{kJ \cdot mol^{-1}}$ is of the same order, and so, the method describes well the system. For the frequencies we observe that all values are overestimated to the experimental ones; can be explained in that our estimates are for harmonic frequencies, when in reality these are anharmonic, because the CO have different constituent, and this breaks the harmonicity, and causes the frequencies to decrease.

8. CONCLUSIONS

From all the data obtained from all the calculations performed, the following conclusions can be withdrawn.

- CO is always adsorbed, and always perpendicular to the surface.
- The adsorption is clearly more stable through the CO C atom.
- Top, Bridge, and Hollow positions can compete are the (001), (011), and (111) surfaces, with no unique, clear trend.
- The strongest adsorption is on (011) surfaces, and the lowest, on (111), and so, the adsorption seems to be biased by the surface coordination and the surface stability.
- Noble metals are the ones that least interact with CO due to their higher stability.
- Ag is more noble than Au, as adsorbs less CO lively due to the deepest energy of the Ag *d*-bands.
- In general, the lower the interaction with CO, the large the distance with respect the surface. The stronger the bond, the close to surfaces and the longer the CO bond length.
- The CO stretching frequencies lower with respect the CO in gas phases and seem dependent on the binding mode; ν (CO) Top> Bridge> Hollow.
- Given the preferential adsorption site, and the different frequencies, are could distinguish different types of CO and surfaces according to simulated IR spectre.

9. REFERENCES AND NOTES

1. Kari, J.; Olsen, J.; Jensen, K.; Badino, S.; Krogh, K.; Borch, K.; Westh, P.; Sabatier Principle for Interfacial (Heterogeneous) Enzyme Catalysis. *ACS Catal*. **2018**, 8, 11966-11972.
2. Andrei, Y. Khodakov; Wei Chu; Pascal, Fongarland; Advances in the Development of Novel Cobalt Fischer−Tropsch Catalysts for Synthesis of Long-Chain Hydrocarbons and Clean Fuels. *Chem. Rev.* **2007**, 107, 1692−1744.
3. G. Pekridis; K. Kalimeri; N. Kaklidis; E. Vakouftsi; E.F. Iliopoulou; C. Athanasio; G.E. Marnellos; V Study of the reverse water gas shift (RWGS) reaction over Pt in a solid oxide fuel cell (SOFC) operating under open and closed-circuit conditions. *Catal Today*. **2007**, 127, 337–346.
4. S.K. Wilkinson; L.G.A. van de Water; B. Miller; M.J.H. Simmons; E.H. Stitt; M.J. Watson. *J CATAL*. **2016**, 337, 208–220.
5. Prabir Basu; Biomass Gasification, Pyrolysis and Torrefaction. Third Edition. Reed, **2002**, p. III-251
6. Mrozek, M; Luo, H; Weaver, M; Formic Acid Electrooxidation on Platinum-Group Metals: Is Adsorbed Carbon Monoxide Solely a Catalytic Poison? *Langmuir*. **2000**,16, 8463-8469.
7. Dong Young Chung; Hyoung-il Kim; Young-Hoon Chung; Myeong Jae Lee; Sung Jong Yoo; Alok D. Bokare; Wonyong Choi; Yung-Eun Sung; Inhibition of CO poisoning on Pt catalyst coupled with the reduction of toxic hexavalent chromium in a dual-functional fuel cell, *Sci Rep.* **2014**.
8. Lorena Vega; Judit Ruvireta; Francesc Viñes; Francesc Illas; Jacob's Ladder as Sketched by Escher: Assessing the Performance of Broadly Used Density Functionals on Transition Metal Surface Properties *J. Phys. Chem.* **2018**, 14, 395–403.
9. Feibelman, P. J.; Hammer, B.; Nørskov, J. K.; Wagner, F.; Scheffler, M.; Stumpf, R.; Watwe, R.; Dumesic, J. The CO/Pt(111)Puzzle. *J. Phys. Chem. B.* **2001**, 105, 4018−4025.
10. Janthon, P.; Kozlov, S.; Viñes, F.; Limtrakul, J.;Illas, F.; Establishing the Accuracy of Broadly Used Density Functionals in Describing Bulk Properties of Transition Metals. *JCTC.* **2013**, 9, 1631-1640.
11. Viñes Solana, F.; Illas i Riera, F.;Sousa Romero, C.; Estudio de la estructura y reactividad de superficies y nanopartículas de carburos de metales de transición. **2008**.
12. Malet, F.; Mirtschink, A.; Giesbertz, K.; Wagner, L.; Gori-Giorgi, P.; Exchange–correlation functionals from the strong interaction limit of DFT: applications to model chemical systems. *J. Phys. Chem.* **2014**, 16, 14551-14558.
13. Yabana, K.; Bertsch, G.; Time-dependent local-density approximation in real time. *PRB,* **1996**, 54, 4484-4487.
14. Ruvireta, J.; Vega, L.;Viñes, F.; Cohesion and coordination effects on transition metal surface energies. *Surf Sci*. **2017**, 664, 45-49.
15. Janthon, P.; Viñes, F.; Sirijaraensre, J.; Limtrakul, J.; Illas, F. Adding Pieces to the CO/Pt(111) Puzzle: The Role of Dispersion. *J. Phys. Chem* . **2017**, 127, 3970-3977.
16. Gao, W.; Abtew, T.; Cai, T.; Sun, Y.; Zhang, S.; Zhang, P.; On the applicability of hybrid functionals for predicting fundamental properties of metals. *Solid State Commun*. **2016**, 234-235,10-13.
17. Kay, K.; IVR Formulation of Miller's Correspondence Relations. *J. Phys. Chem.* **2001**, 105, 2535-2545.
18. Halstead, J.; Teaching the Spin Selection Rule: An Inductive Approach. *J. Phys. Chem.* **2012**, 90,70-75.

19. Blöchl, P.; *E. Phys. Rev. B **1994**, 50, 17953.*
20. Vega, L.; Martínez, B.; Viñes, F. and Illas, F.; Robustness of surface activity electronic structure-based descriptors of transition metals, *PCCP*. **2018**, 20,20548-20554.
21. Viñes, F.; Konstantatos, G.; Illas, F.; Matildite Contact with Media: First-Principles Study of AgBiS2 Surfaces and Nanoparticle Morphology. *J. Phys. Chem.* **2017**, 122, 521-526.
22. Piqué, O.; Koleva, I.; Viñes, F.; Aleksandrov, H.; Vayssilov, G.; Illas, F.; Subsurface Carbon – a General Feature of Noble Metals. *Angew. Chem*.**2018.**
23. Gajdo, M.; Eichler, A.; Hafner, J.; CO adsorption on close-packed transition and noble metal surfaces: trends fromab initiocalculations. *J. Phys. Chem: Condensed Matter.* **2004**, 16, 1141-1164.German,
24. Koch, H.; Singnurkar, P.; Schennach, R.; Stroppa, A.; Mittendorfer, F.; A RAIRS, TPD, and DFT Study of Carbon Monoxide Adsorption on Stepped Rh (553). *J. Phys. Chem*. **2008**, 112, 806-812.
25. Sheintuch, M.; Comparative Theoretical Study of CO Adsorption and Desorption Kinetics on (111) Surfaces of Transition Metals. *J. Phys. Chem*. **2008**, 112, 14377-14384.
26. Hsing, C.; Chang, C., Cheng, C.; Wei, C.; Quantum Monte Carlo Studies of CO Adsorption on Transition Metal Surfaces. *J. Phys. Chem.* **2019**.
27. Karmakar, S.; Chowdhury, C.; Datta, A.; Noble-Metal-Supported GeS Monolayer as Promising Single-Atom Catalyst for CO Oxidation. *J. Phys. Chem.*. **2018**, 122,14488-14498.
28. Wellendorff, J.; Silbaugh, T.; Garcia-Pintos, D.; Nørskov, J., Bligaard, T.; Studt, F.; Campbell, C. A benchmark database for adsorption bond energies to transition metal surfaces and comparison to selected DFT functionals. *Surf Sci.* **2015**, 640, 36-44.